CASE FILE
COPY

NACA

RESEARCH MEMORANDUM

COMPARISON OF ZERO-LIFT DRAGS DETERMINED BY FLIGHT TESTS AT TRANSONIC SPEEDS OF SYMMETRICALLY MOUNTED NACELLES IN VARIOUS SPANWISE POSITIONS ON A 45° SWEPTBACK WING AND BODY COMBINATION

By William B. Pepper, Jr., and Sherwood Hoffman

Langley Aeronautical Laboratory
Langley Field, Va.

NATIONAL ADVISORY COMMITTEE
FOR AERONAUTICS

WASHINGTON
May 23, 1951

NATIONAL ADVISORY COMMITTEE FOR AERONAUTICS

RESEARCH MEMORANDUM

COMPARISON OF ZERO-LIFT DRAGS DETERMINED BY FLIGHT TESTS AT TRANSONIC SPEEDS OF SYMMETRICALLY MOUNTED NACELLES IN VARIOUS SPANWISE POSITIONS ON A 45° SWEPTBACK WING AND BODY COMBINATION

By William B. Pepper, Jr., and Sherwood Hoffman

SUMMARY

Rocket-powered models were flown at transonic speeds to determine the effect of nacelle location on zero-lift drag. Symmetrically mounted nacelles of fineness ratio 9.66 were successively located spanwise at 18, 25, 40, 60, 80, and 96 percent of the wing semispan. The chordwise location of the nacelles was such that approximately 50 percent of the nacelle length was forward of the wing maximum thickness. The wing had a sweepback angle of 45° along the quarter-chord line, an aspect ratio of 6.0, a taper ratio of 0.6, and an NACA 65A009 airfoil section in the free-stream direction. The fuselage fineness ratio was 10.0.

For the present wing-body-nacelle configuration, low drag was obtained for all the spanwise nacelle positions at Mach numbers between 0.80 and 0.91. Nacelles mounted at the wing tips gave the lowest drag throughout the transonic speed range. For this nacelle location the drag was lower than the drag of the test configuration without nacelles over most of the speed range. The inboard nacelle position showed low drag throughout most of the transonic region. Intermediate nacelle positions on the wing gave the highest drag. The force-break Mach number of the wing-body-fin combination was not appreciably reduced by placing nacelles near the wing tips or near the fuselage. Other locations reduced the force-break Mach number as much as 0.05.

INTRODUCTION

As part of a general transonic research program of the National Advisory Committee for Aeronautics to determine the aerodynamic properties of promising aircraft configurations, the Langley Pilotless Aircraft Research Division at Wallops Island, Va., has tested a series of rocket-propelled free-flight models to determine the variations of zero-lift drag coefficient for a transonic configuration of high aspect ratio with nacelles at various positions on the wings.

Interference drag at subsonic speeds for many types of configurations with different wing-body-nacelle combinations has been investigated experimentally and theoretically. Owing to the complexities encountered in theoretical studies, the determination of transonic interference effects has been made solely through experiment. The initial investigations of such interference effects were confined to models with low-aspect-ratio wings. Presently, the importance of the high-speed long-range airplane has led to the exploration at transonic speeds of interference effects of wing-body-nacelle combinations having high-aspect-ratio wings.

The wing-body configuration used for the tests covered in this paper was the same as the configuration used in the chordwise nacelle position tests of reference 1. This configuration is believed to be practical for transonic flight because of its low drag coefficient and high force-break Mach number, which was well above 0.9. The wing had a sweepback angle of 45° along the quarter-chord line, an aspect ratio of 6.0, a taper ratio of 0.6, and an NACA 65A009 airfoil section in the free-stream direction. The low-drag fuselage had a fineness ratio of 10.0 and was a modification of a fuselage developed by the NACA from free-fall tests.

A twin-engine airplane was assumed in order to study individual nacelle interference. The size of the nacelle was determined from the consideration that the full-scale nacelle represented was 50 inches in diameter on a wing of 1500 square feet of area. A nacelle fineness ratio of 9.66 was selected to accommodate an axial-flow turbojet engine with an afterburner.

The tests were conducted without air flow through the nacelles to simplify the investigation. It is anticipated, however, that, with the introduction of internal air flow, the resulting variations of drag with ducted-nacelle location would be similar to the variations found for solid nacelles. Accordingly, the nacelle was made solid by fairing the nacelle curvature from the air inlet to a pointed nose.

From the results of reference 1, a favorable chordwise location was selected at the 40-percent semispan station. The nacelles then were varied along the wing span with the pointed nose of each nacelle kept at a constant distance ahead of the maximum wing thickness at the local wing chord.

Tests covered a continuous Mach number range from 0.80 to 1.25. The Reynolds number was based on the mean aerodynamic chord and varied from 3.8×10^6 to 7.6×10^6 over the speed range.

SYMBOLS

a	longitudinal acceleration, feet per second per second
b	wing span, feet
C_D	total drag coefficient, based on S_W
C_{D_N}	drag coefficient for nacelle plus interference, based on S_F
g	acceleration due to gravity, 32.2 feet per second per second
M	Mach number $\left(V/V_c\right)$
q	free-stream dynamic pressure, pounds per square foot
R	Reynolds number, based on wing mean aerodynamic chord
S_F	frontal area of one nacelle, square feet
S_W	total wing plan-form area, square feet
V	velocity along flight path, feet per second
V_c	speed of sound, feet per second
W	model weight after burnout, pounds
γ	flight-path angle, degrees
x	station, inches

Y wing semispan station, measured from fuselage center line

y ordinate, inches

MODELS

Details and dimensions of the wing-body-fin combination and the solid nacelle are given in figures 1 to 3 and tables I to III. Photographs showing the general arrangements of the models flown are presented as figure 4.

The models employed for this investigation were the same as those in reference 1 except for the location of the nacelles. The fuselage of reference 2 was reduced from a fineness ratio of 12 to 10 by cutting off the rear one-sixth of the body. In order to fit a 3.25-inch Mk. 7 aircraft rocket motor into this body, the rear 28 percent of the modified body was enlarged. The frontal area of the fuselage was 0.242 square foot.

The wing had a sweepback angle of 45° along the quarter-chord line, an aspect ratio of 6.0 based on the total wing-plan-form area of 3.878 square feet, a taper ratio of 0.6, and an NACA 65A009 airfoil in the free-stream direction. The leading edge of the wing intersected the fuselage at the maximum diameter. The ratio of total wing-plan-form area to the fuselage frontal area was 16.0.

The nacelles were bodies of revolution having a fineness ratio of 9.66 and a frontal area of 0.034 square foot. Each nacelle was designed to have an NACA 1-50-250 nose-inlet profile (based on data in reference 3), a cylindrical midsection, and an afterbody of NACA 111 proportions (reference 4). For this investigation, the method of conical lofting from reference 5 was used to design a nose plug to close off the nacelle inlet.

The center lines of the nacelles were in the wing plane parallel to the free-stream direction and were located at 0.18, 0.25, 0.40, 0.60, 0.80, and 0.96 wing semispans measured from the center line of the fuselage. At the 0.96 station, the outside edge of the nacelle was made flush with the tip of the wing. The distance between the pointed nose of the nacelle and the maximum thickness of the local wing chord (40-percent-chord line) was kept constant at 11.45 inches for all the models. This arrangement was determined to be a favorable nacelle location at 40 percent of the semispan from reference 1. No filleting was employed at the nacelle-wing junctures.

Two vertical fins were used to stabilize the model directionally. No fins were required in the horizontal plane because the sweptback wing was located far enough rearward on the fuselage to stabilize the model in this plane (fig. 1). The leading edges of the fins were swept back 45° and the fins were 0.091 inch thick. The exposed plan-form area of the two fins was 0.468 square foot.

TESTS AND MEASUREMENTS

Flight tests at zero lift covered a Reynolds number range, based on wing mean aerodynamic chord, from 3.8×10^6 at $M = 0.8$ to 7.6×10^6 at $M = 1.3$ as shown in figure 5. The possible error was established from three similar models in reference 1 and was based on the maximum deviation found between faired curves of the experimental drag points. The error in the total drag coefficient, based on total wing-plan-form area of 3.878 square feet, was within ±0.0004. For the nacelle-plus-interference drag coefficient, based on 0.034-square-foot nacelle frontal area, the error was within ±0.046.

Each model was propelled by a two-stage rocket system and launched from a rail launcher (fig. 4(a)). The first stage consisted of a 5-inch light-weight high-velocity aircraft rocket motor that served to accelerate the model from zero velocity to high-subsonic speeds. For the second stage, a 3.25-inch Mk. 7 aircraft rocket motor was installed in the fuselage to accelerate the model to supersonic speeds. Tracking instrumentation consisting of a C. W. Doppler velocimeter and an NACA modified SCR-584 tracking unit was used to determine the deceleration and flight path during coasting flight. A survey of atmospheric conditions at the time of each launching was made through radiosonde measurements from an ascending balloon.

The values of drag coefficient, based on total wing-plan-form area, were calculated by using the formula

$$C_D = -\frac{W}{qgS_W}(a + g \sin \gamma)$$

The nacelle-plus-interference drag coefficient was obtained from the differences in drag between a model without nacelles and a model with nacelles. This coefficient, based on nacelle frontal area, is

$$C_{D_N} = \left(C_{D_{\text{nacelles on}}} - C_{D_{\text{nacelles off}}}\right)\frac{S_W}{2S_F}$$

RESULTS AND DISCUSSION

The variations of total drag coefficient with Mach number for all the models tested are given in figure 6 and are summarized in figure 7.

From a comparison of the curves of C_D against M in figure 7, it is evident that the wing-tip nacelle location (model F) was the best position tested. Between $M = 0.80$ and $M = 0.91$, C_D for models A to E was approximately equal to C_D of the model without nacelles. The drag coefficient of model F, however, was lower in this speed range, with its minimum drag coefficient at $M = 0.90$. At this Mach number, C_D of model F is 13 percent lower than the drag coefficient of the model without nacelles.

Between $M = 0.90$ and $M = 1.00$, the drag coefficients of all the models increased sharply about 100 to 150 percent. The Mach number at which the drag rise occurred was about 0.05 higher for models with nacelles located in the proximity of the wing tips or fuselage than for models having nacelles located near the middle of the semispan. The drag-rise Mach number of 0.96 for the wing-body combination was not noticeably reduced by adding nacelles near the wing tips.

The addition of nacelles at all spanwise positions, except at the tip, increased the C_D at Mach numbers greater than 1.0. By adding nacelles at the wing tips, the drag of the wing-body combination was reduced up to $M = 1.09$. Above this Mach number, the drag coefficient was slightly higher than that for the wing-body combination. Nacelles located in midsemispan positions were observed to have the highest increase in drag coefficient.

The variations with Mach number of nacelle-plus-interference drag coefficient C_{D_N} for all the nacelle positions investigated are given in figure 6. An estimated drag coefficient for an isolated nacelle (using the results of reference 1) is also plotted so that the interference drag may be approximated. Favorable interference is indicated for nacelles located at 0.18, 0.80, and 0.96 of the semispan. For the other nacelle positions, unfavorable interference is present near Mach number 1.

Values of C_{D_N} are cross plotted with respect to spanwise nacelle location and Mach number in figure 8. Contour lines, representing lines of constant C_{D_N}, are drawn through experimental points. Nacelle positions on the wing-body-nacelle configurations used herein may be

selected from figure 8 for low drag over a desired speed range. Up to $M = 0.91$, these nacelles may be located at any spanwise position on the wing. In order to obtain low drag at higher Mach numbers, it is evident that the nacelles should be located near the wing tip or near the fuselage.

CONCLUSIONS

The effect on drag of varying the spanwise position of nacelles on a 45° sweptback wing and body combination has been determined through transonic flight tests at zero lift. The pointed nose of each nacelle was located at a constant distance ahead of the line of maximum wing thickness. The following effects were noted:

1. Low drag was obtained between $M = 0.80$ and $M = 0.91$ for all the nacelle positions investigated.

2. Nacelles located at the wing tips gave the lowest drag, which was less than the drag of the wing-body-fin configuration without nacelles over most of the speed range. Intermediate nacelle positions on the wing gave the highest drag.

3. The force-break Mach number of the wing-body-fin combination was not appreciably reduced by mounting nacelles near the wing tips or near the fuselage. Other locations reduced the force-break Mach number as much as 0.05.

4. Favorable interference between the nacelle and wing body was indicated over the test Mach number range for the 18, 80, and 96 percent semispan locations of the wing.

Langley Aeronautical Laboratory
National Advisory Committee for Aeronautics
Langley Field, Va.

REFERENCES

1. Pepper, William B., Jr., and Hoffman, Sherwood: Transonic Flight Tests to Compare the Zero-Lift Drag of Underslung and Symmetrical Nacelles Varied Chordwise at 40 Percent Semispan of a 45° Swept-back, Tapered Wing. NACA RM L50G17a, 1950.

2. Thompson, Jim Rogers: Measurements of the Drag and Pressure Distribution on a Body of Revolution throughout Transition from Subsonic to Supersonic Speeds: NACA RM L9J27, 1950.

3. Baals, Donald D., Smith, Norman F., and Wright, John B.: The Development and Application of High-Critical-Speed Nose Inlets. NACA Rep. 920, 1948.

4. Abbott, Ira H.: Fuselage-Drag Tests in the Variable-Density Wind Tunnel: Streamline Bodies of Revolution, Fineness Ratio of 5. NACA TN 614, 1937.

5. Dannenberg, Robert E.: The Development of Jet-Engine Nacelles for a High-Speed Bomber Design. NACA RM A7D10, 1947.

TABLE I

FUSELAGE COORDINATES

x (in.)	y (in.)
0	0
.4	.185
.6	.238
1.0	.342
2.0	.578
4.0	.964
6.0	1.290
8.0	1.577
12.0	2.074
16.0	2.472
20.0	2.772
24.0	2.993
28.0	3.146
32.0	3.250
36.0	3.314
40.0	3.334
44.0	3.304
48.0	3.219
52.0	3.037
56.0	2.849
60.0	2.661
64.0	2.474
66.7	2.347

NACA

TABLE II

COORDINATES OF NACA 65A009 AIRFOIL

x/c (percent)	y/c (percent)
0	0
.5	.688
.75	.835
1.25	1.065
2.5	1.460
5.0	1.964
7.5	2.385
10.0	2.736
15.0	3.292
20.0	3.714
25.0	4.036
30.0	4.268
35.0	4.421
40.0	4.495
45.0	4.485
50.0	4.377
55.0	4.169
60.0	3.874
65.0	3.509
70.0	3.089
75.0	2.620
80.0	2.117
85.0	1.594
90.0	1.069
95.0	.544
100.0	.019
L.E. radius: 0.58 percent c	

TABLE III

COORDINATES FOR SOLID NACELLE

x (in.)	y (in.)
0	0
.100	.070
.330	.169
.830	.336
1.330	.489
1.830	.622
2.330	.747
2.580	.800
2.958	.876
3.585	.974
4.840	1.105
6.095	1.190
7.350	1.240
8.605	1.255
16.830	1.255
17.872	1.237
18.913	1.195
19.955	1.127
20.996	1.029
22.038	.909
23.079	.768
24.121	.616
24.250	.598

NACA

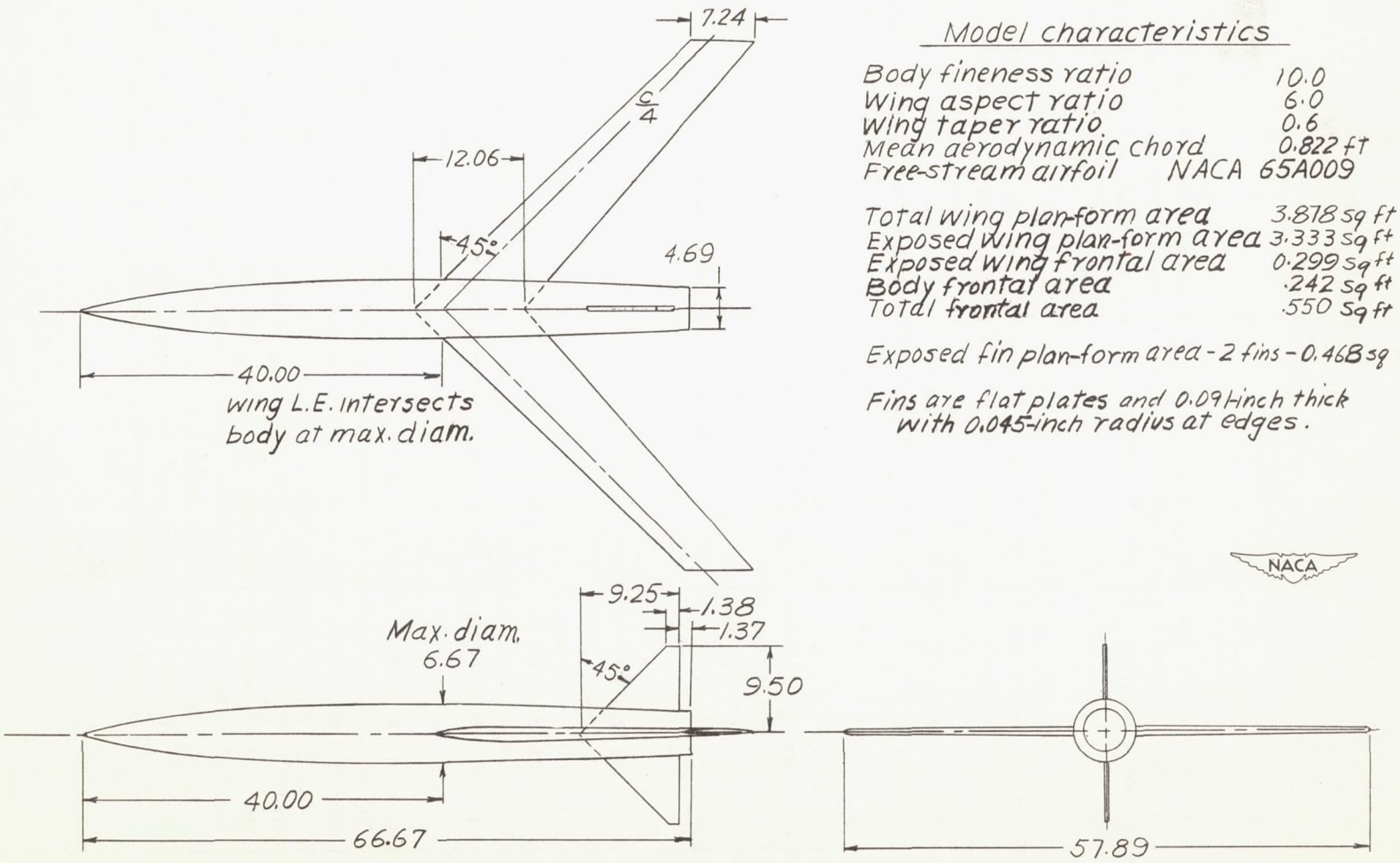

Model characteristics

Body fineness ratio	10.0
Wing aspect ratio	6.0
Wing taper ratio	0.6
Mean aerodynamic chord	0.822 ft
Free-stream airfoil	NACA 65A009
Total wing plan-form area	3.878 sq ft
Exposed wing plan-form area	3.333 sq ft
Exposed wing frontal area	0.299 sq ft
Body frontal area	.242 sq ft
Total frontal area	.550 sq ft

Exposed fin plan-form area - 2 fins - 0.468 sq ft

Fins are flat plates and 0.091-inch thick with 0.045-inch radius at edges.

Figure 1.- General arrangement and dimensions of test model. All dimensions are in inches.

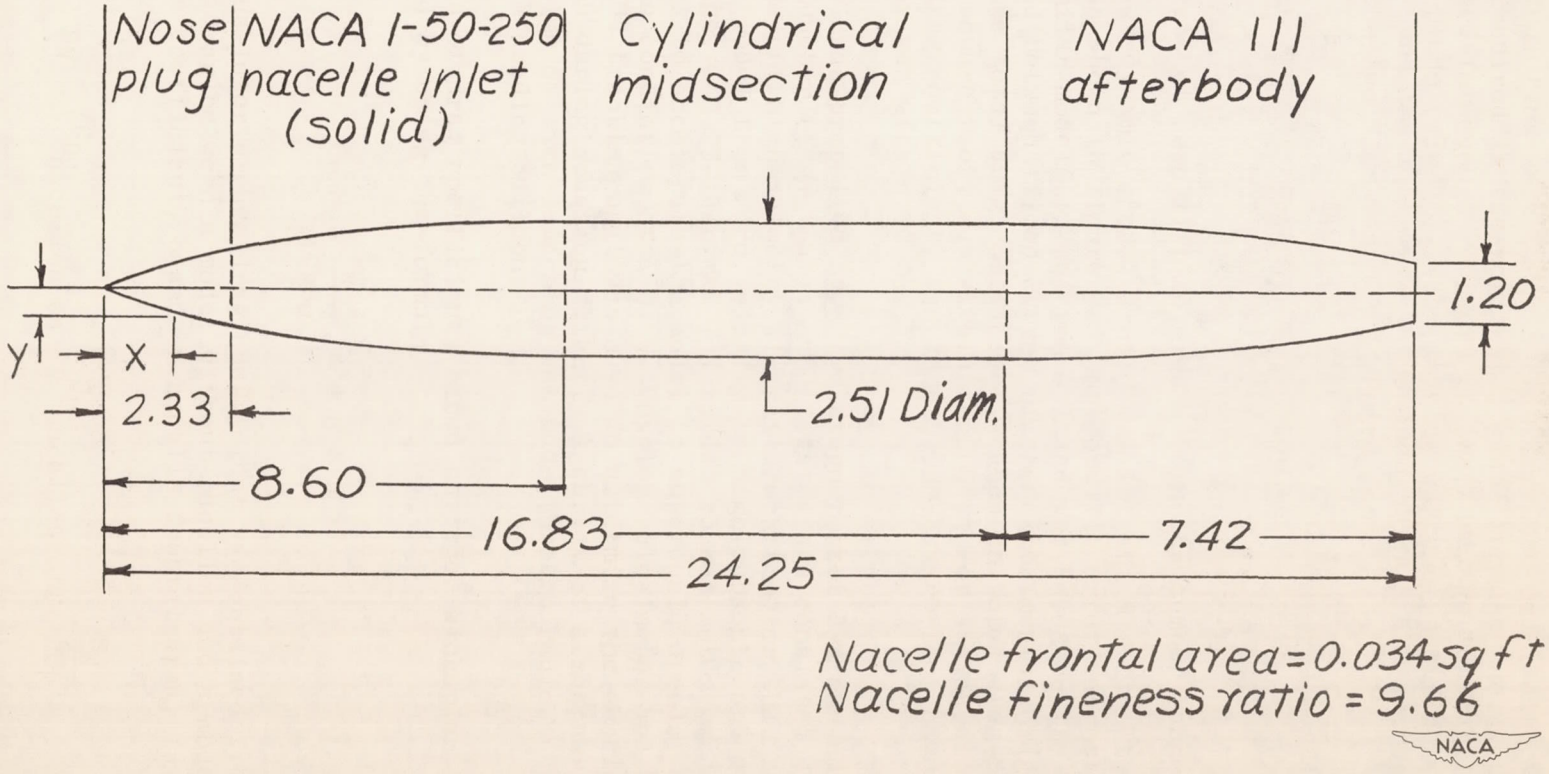

Figure 2.- Details and dimensions of nacelle. All dimensions are in inches.

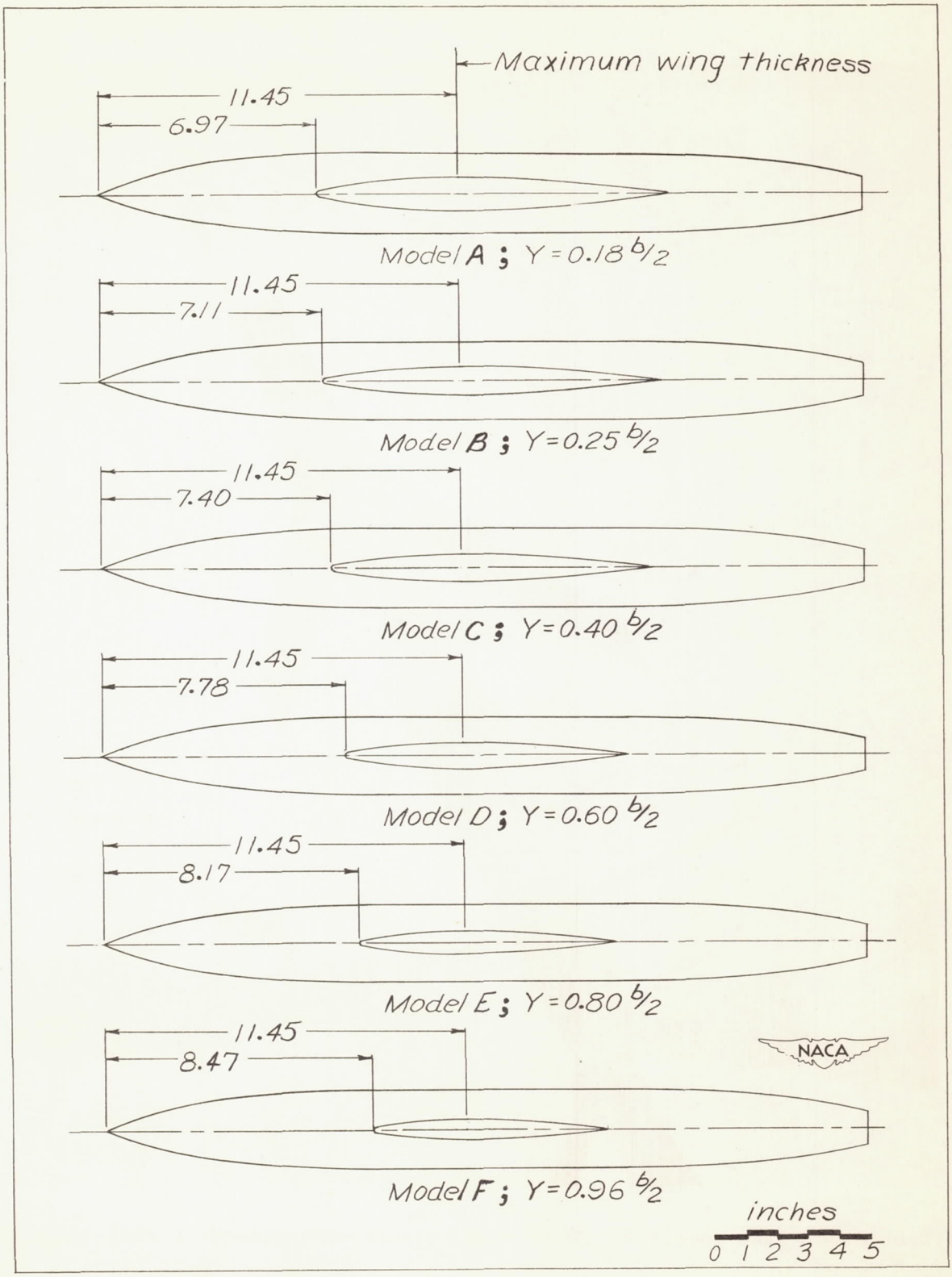

Figure 3.- Sectional views of nacelle location along semispan.

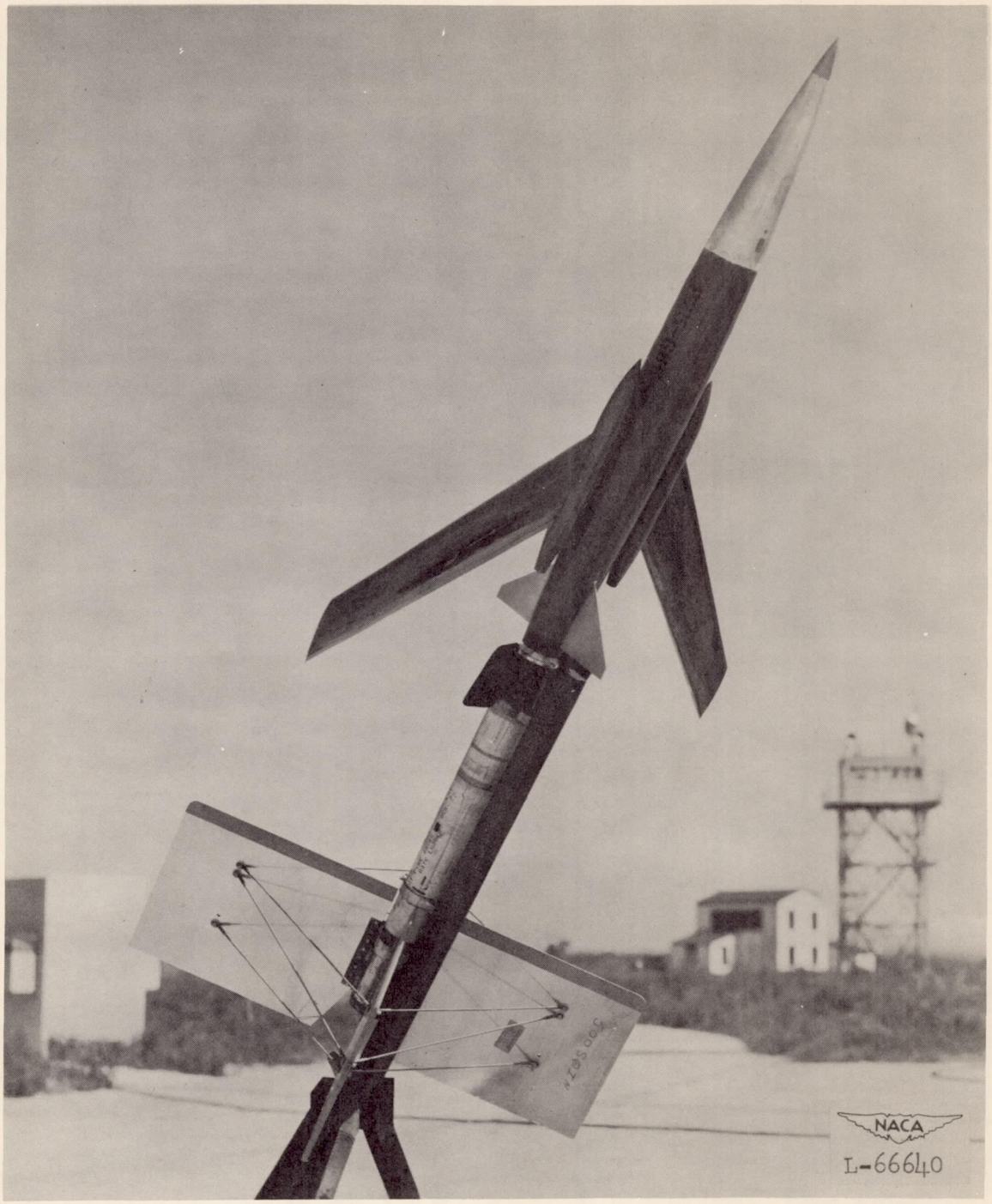

(a) Test model with nacelles. Model and booster arrangement in rail launcher.

Figure 4.- General views of test models.

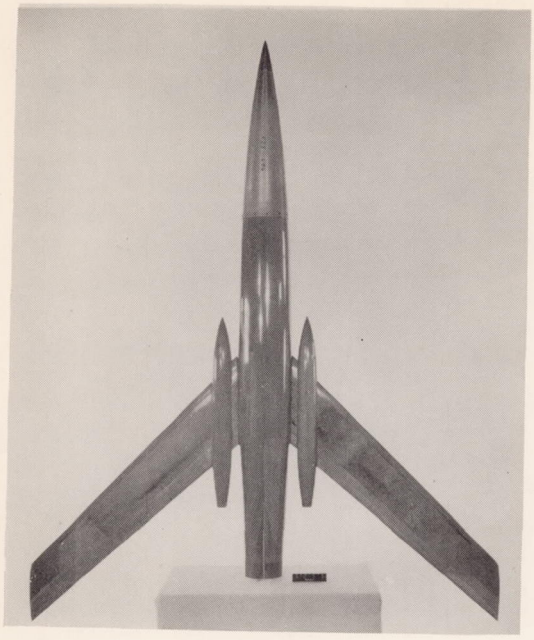

Model A; Y = 0.18b/2

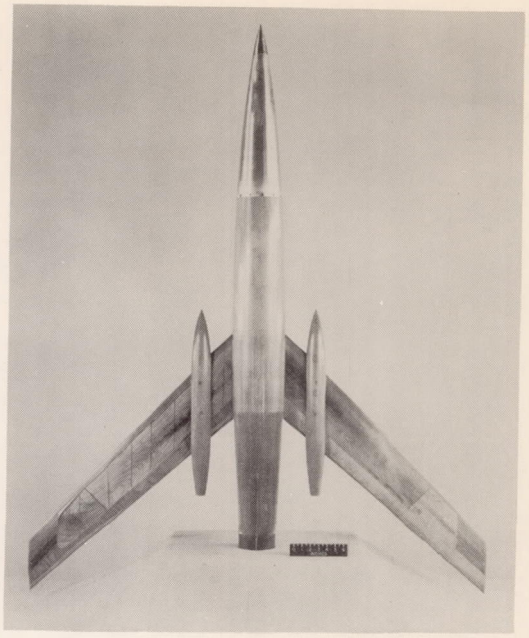

Model B; Y = 0.25b/2

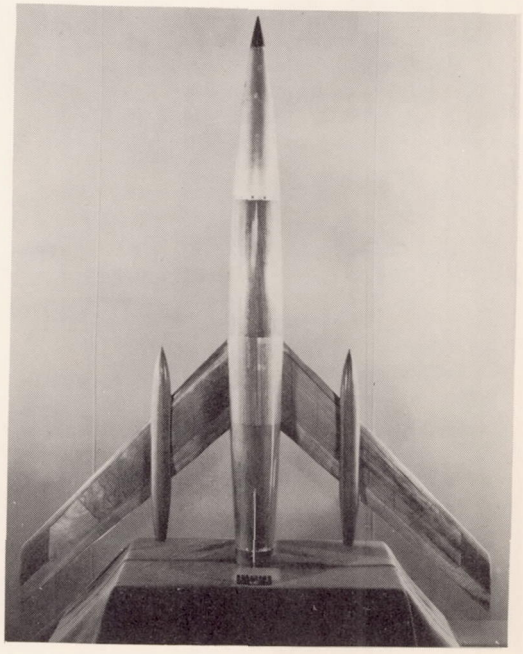

Model C; Y = 0.40b/2

(b) Models with nacelles located inboard on the wing.

L-69123

Figure 4.- Continued.

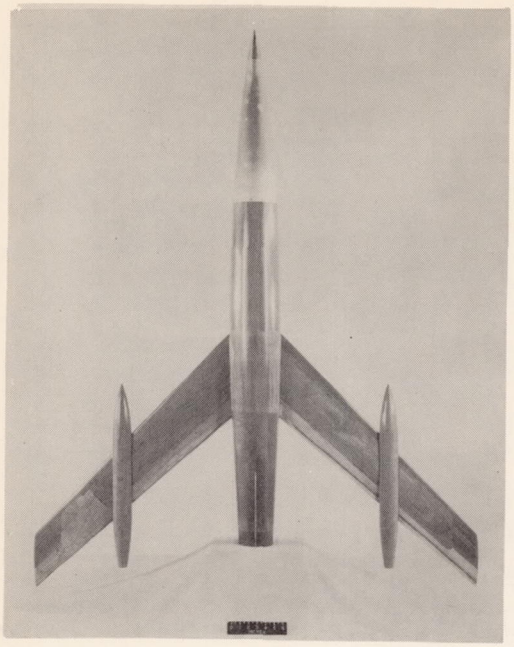

Model D; Y = 0.60b/2

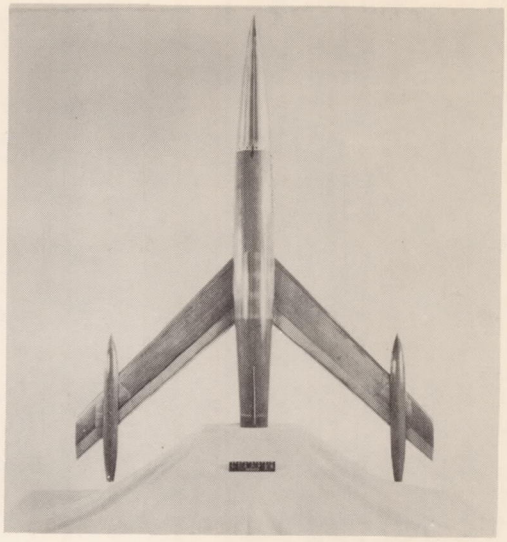

Model E; Y = 0.80b/2

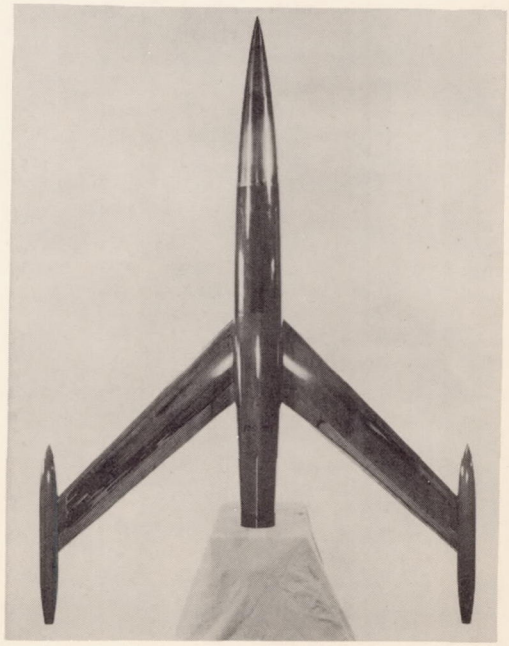

Model F; Y = 0.96b/2

(c) Models with nacelles located outboard on the wing.

L-69124

Figure 4.- Concluded.

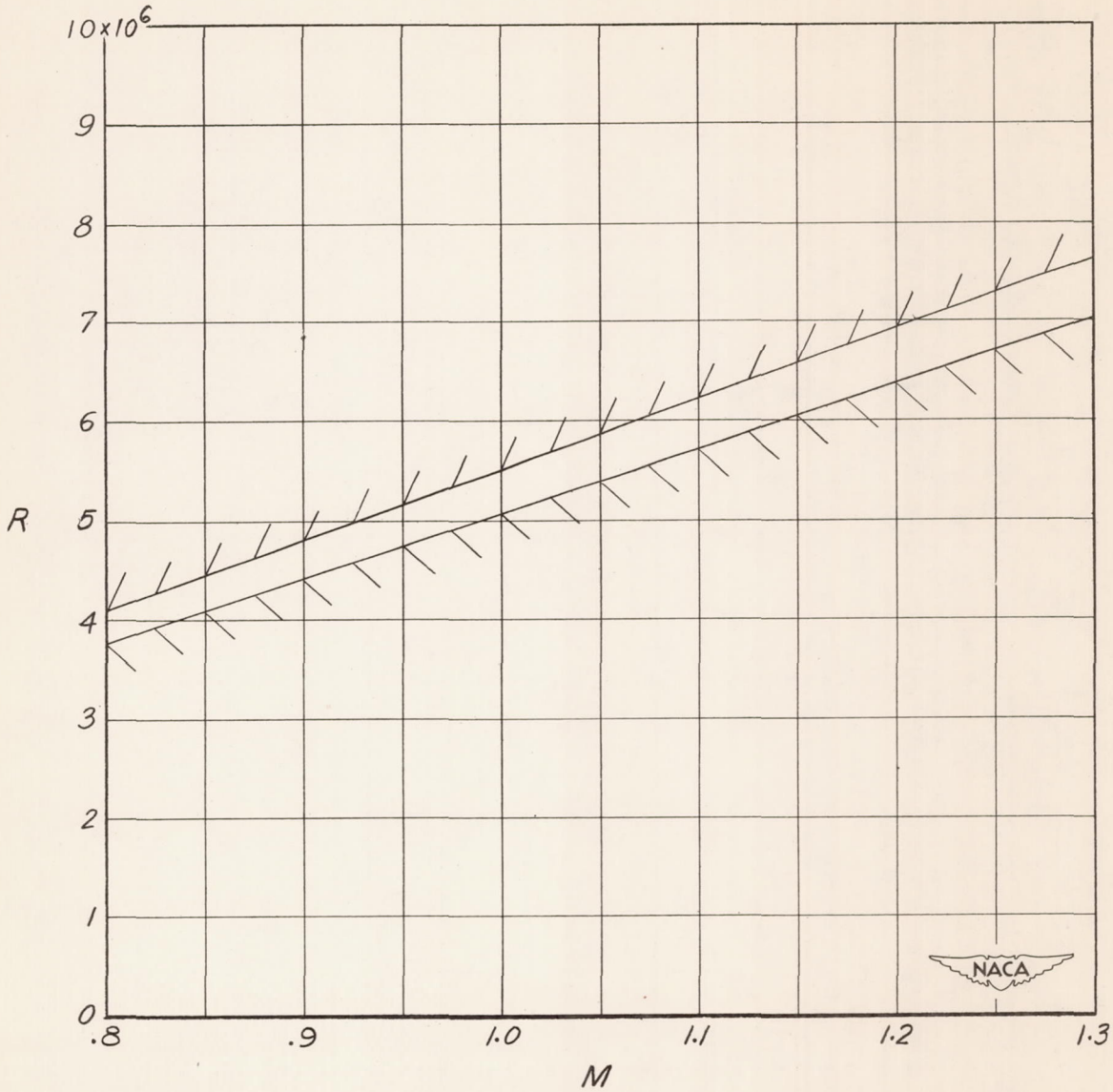

Figure 5.- Variation of Reynolds number range with Mach number for models tested. Reynolds number based on mean aerodynamic wing chord.

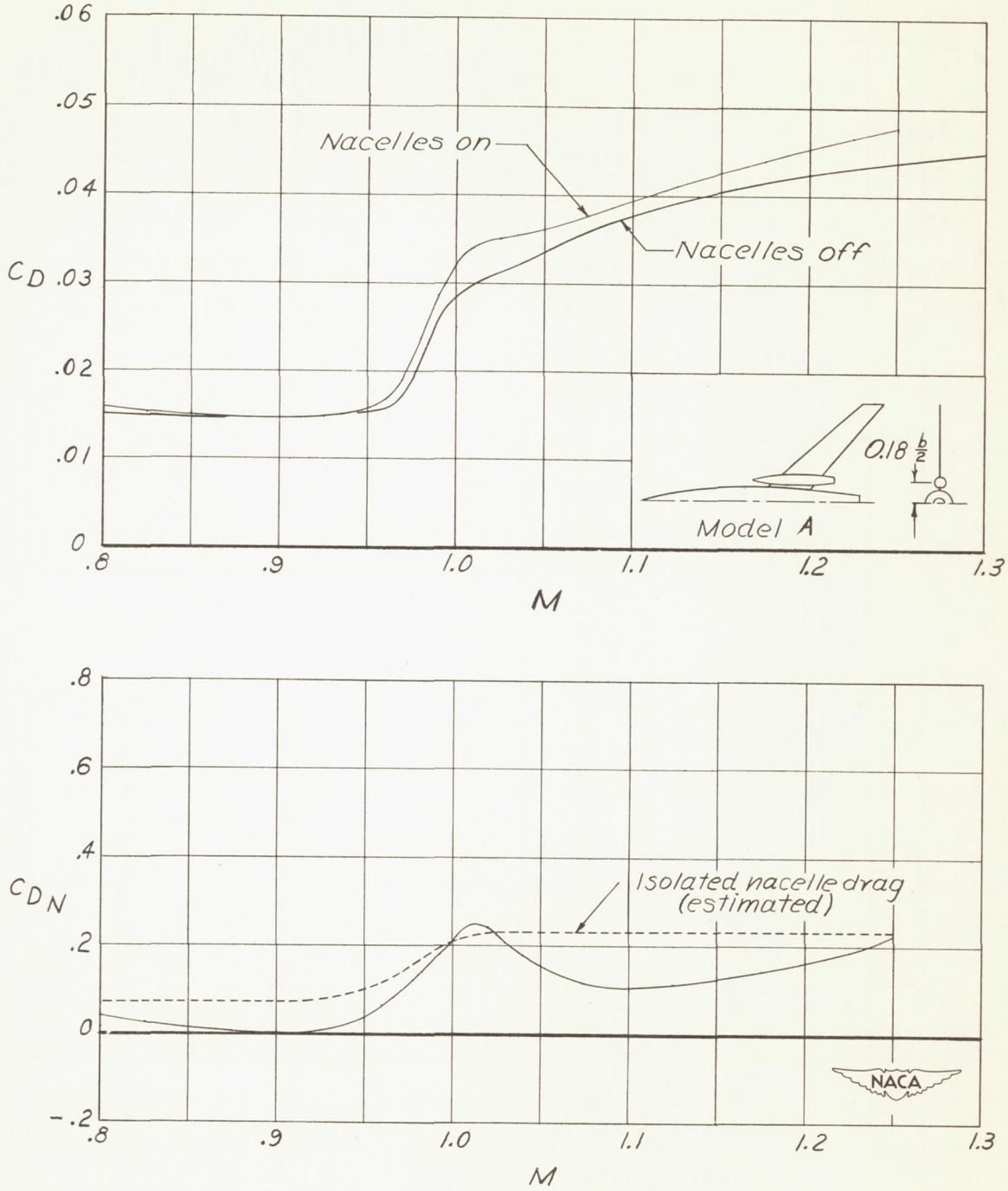

(a) Nacelles located at the wing 0.18 semispan station.

Figure 6.- Variations of total drag, wing-body drag, and nacelle drag coefficients with Mach number.

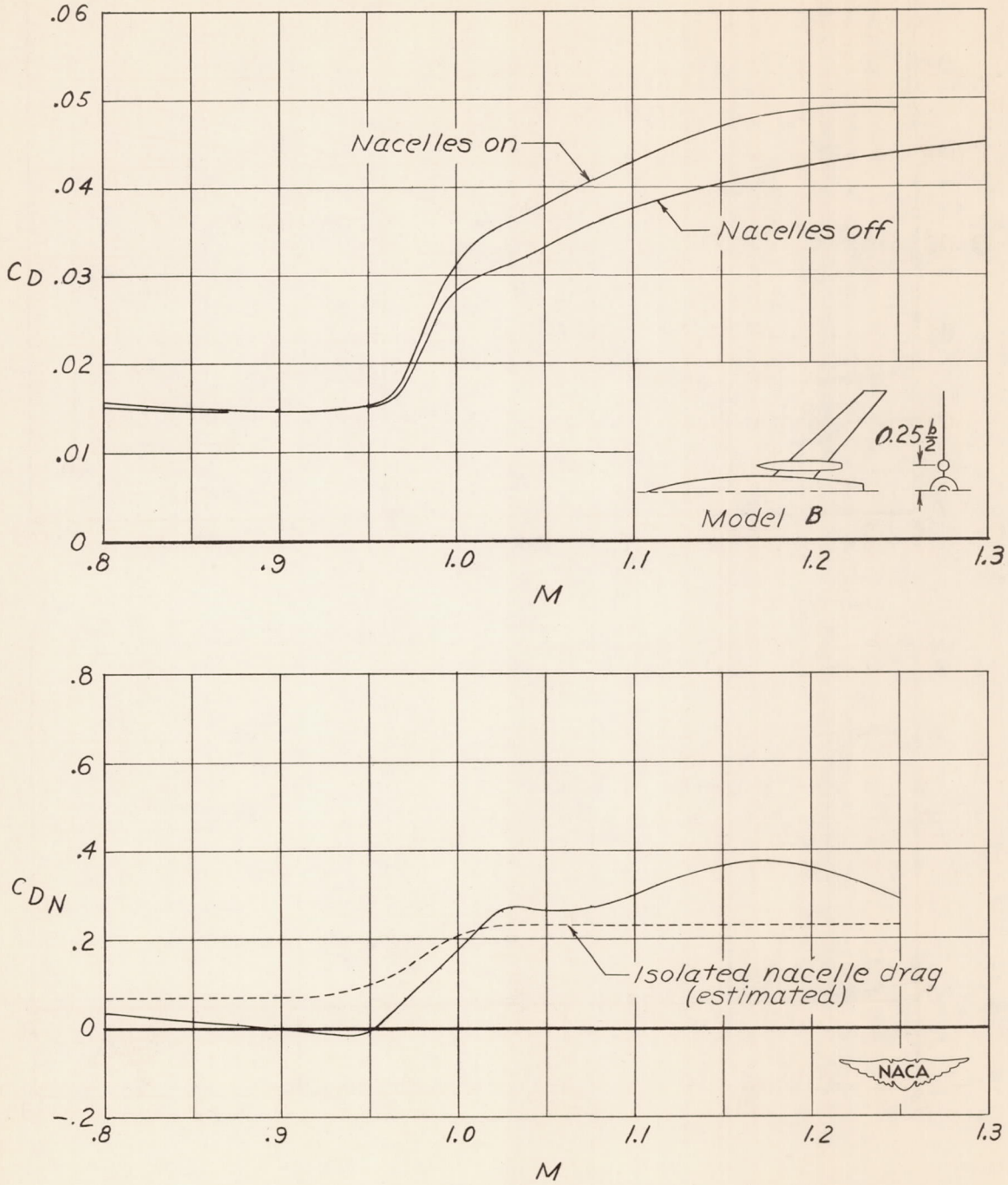

(b) Nacelles located at the wing 0.25 semispan station.

Figure 6.- Continued.

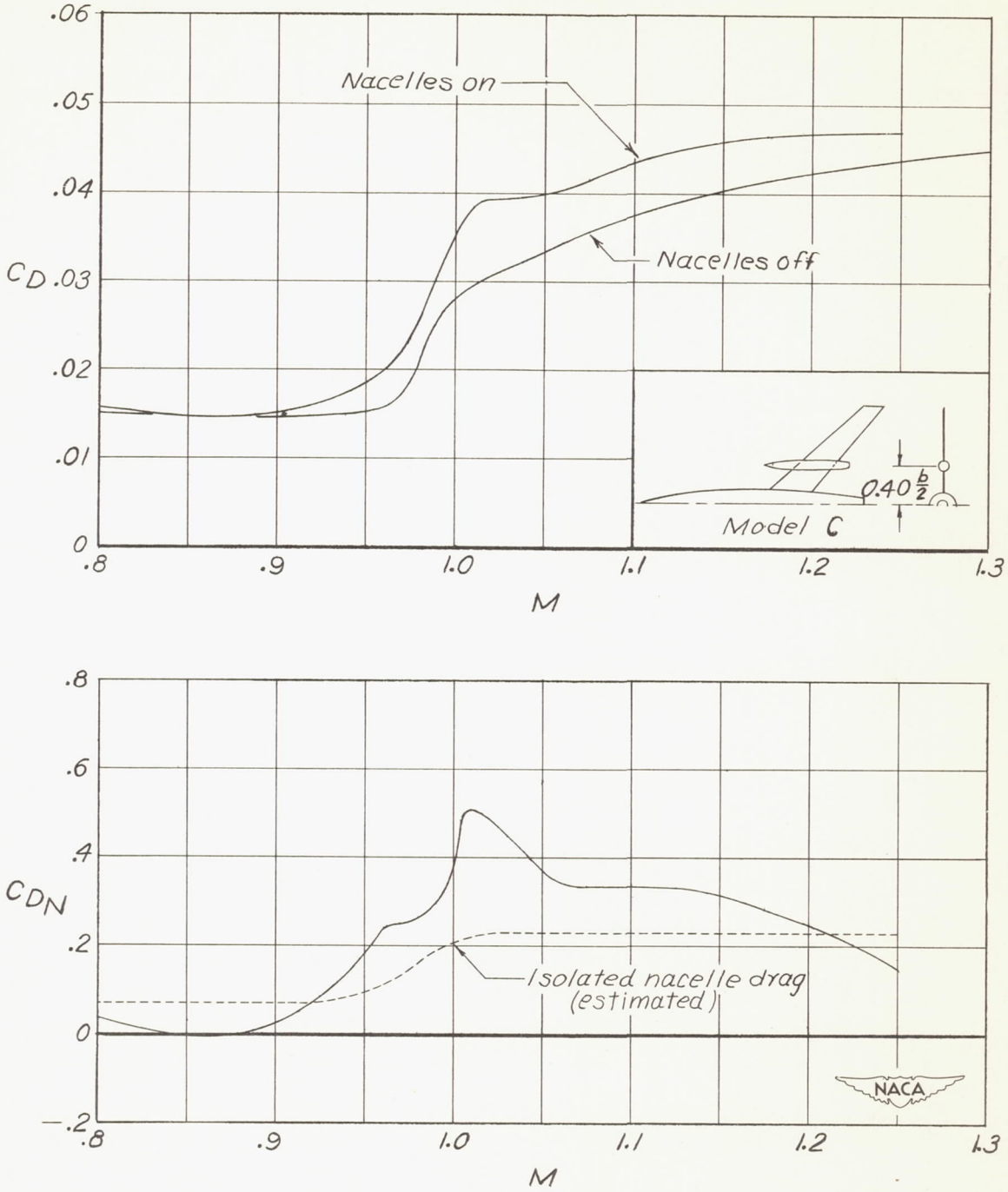

(c) Nacelles located at the wing 0.40 semispan station.

Figure 6.- Continued.

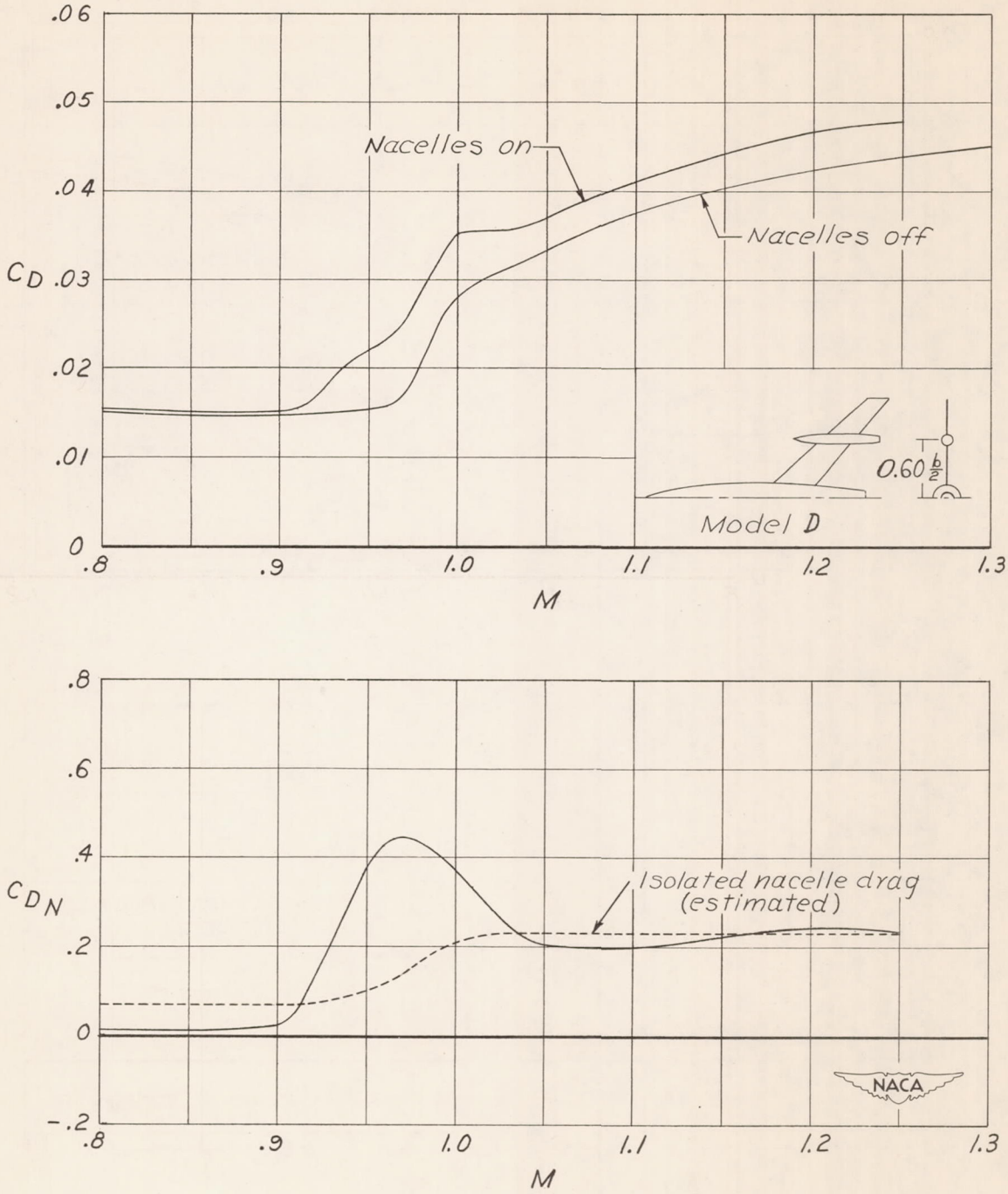

(d) Nacelles located at the wing 0.60 semispan station.

Figure 6.- Continued.

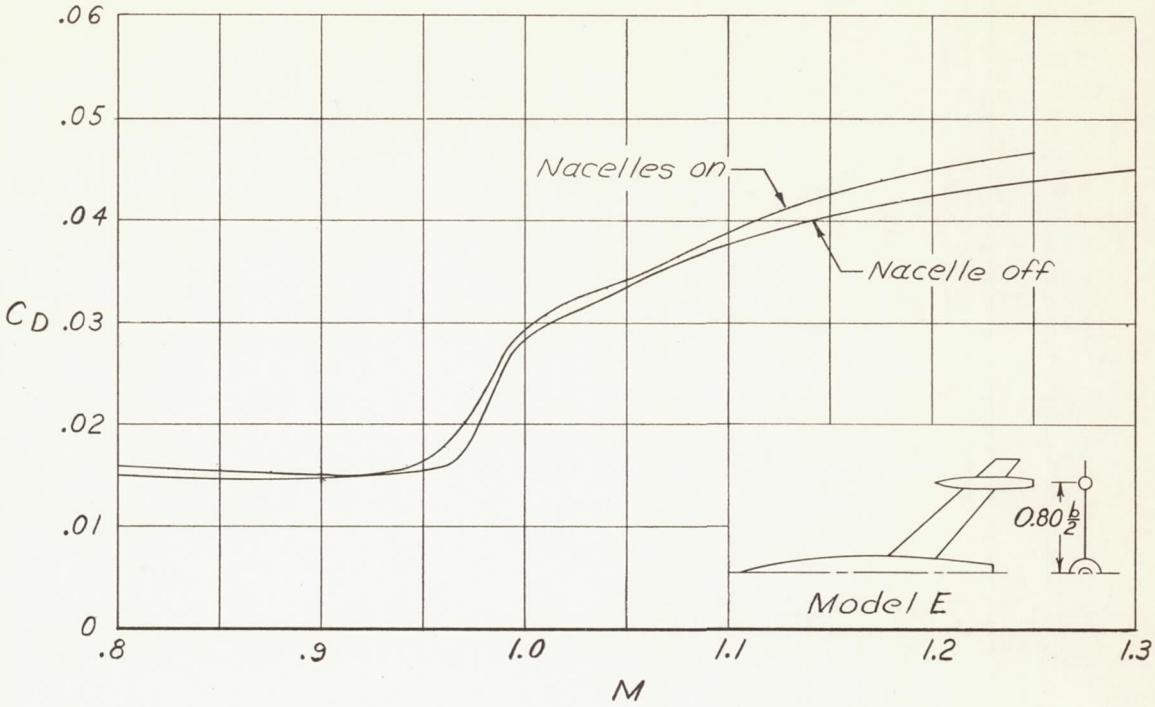

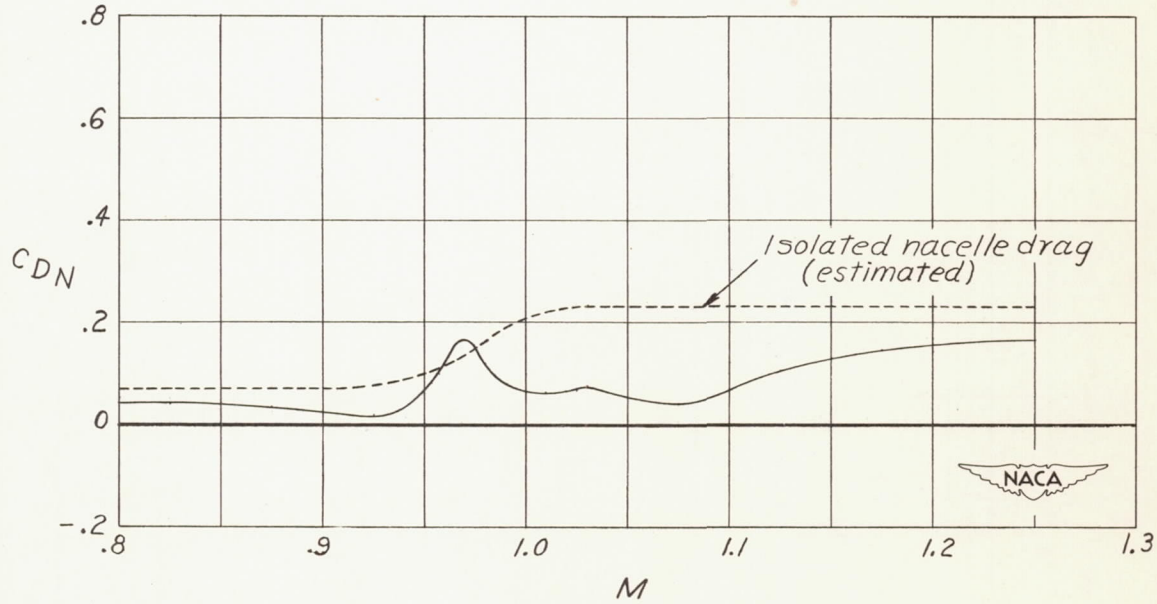

(e) Nacelles located at the wing 0.80 semispan station.

Figure 6.- Continued.

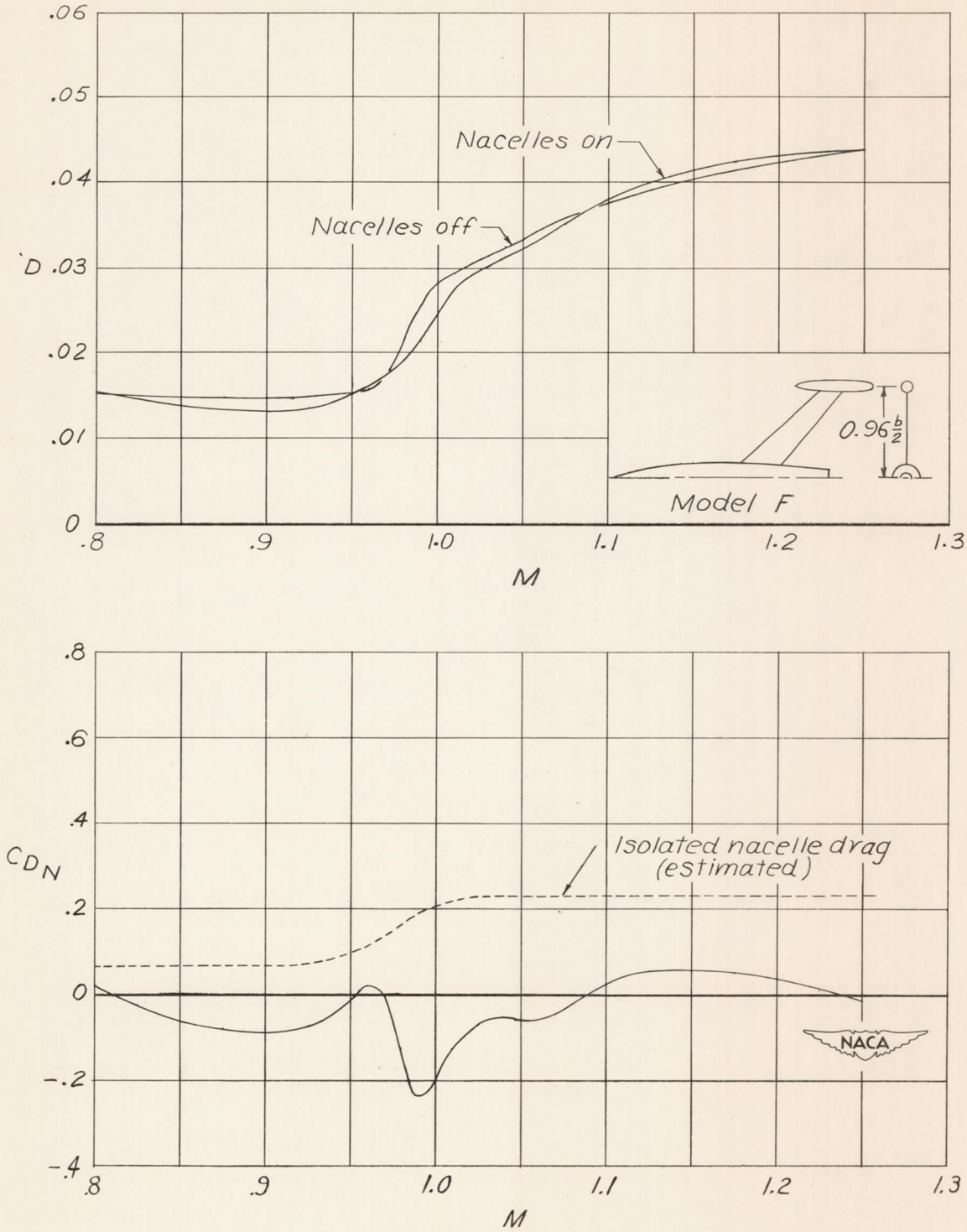

(f) Nacelles located at the wing 0.96 semispan station.

Figure 6.- Concluded.

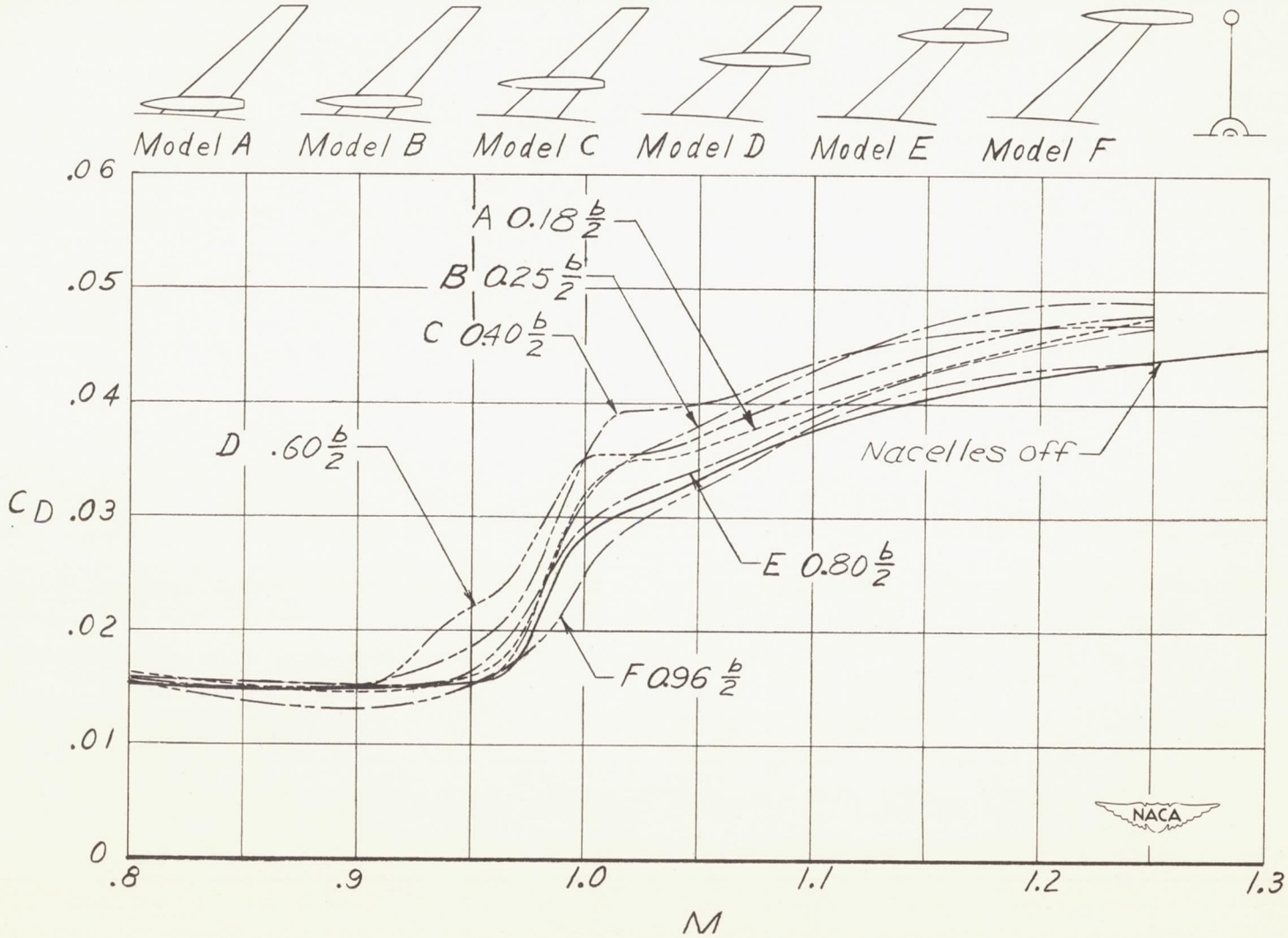

Figure 7.- Comparison of total drag coefficients for models with nacelles in various spanwise positions along the wing semispan.

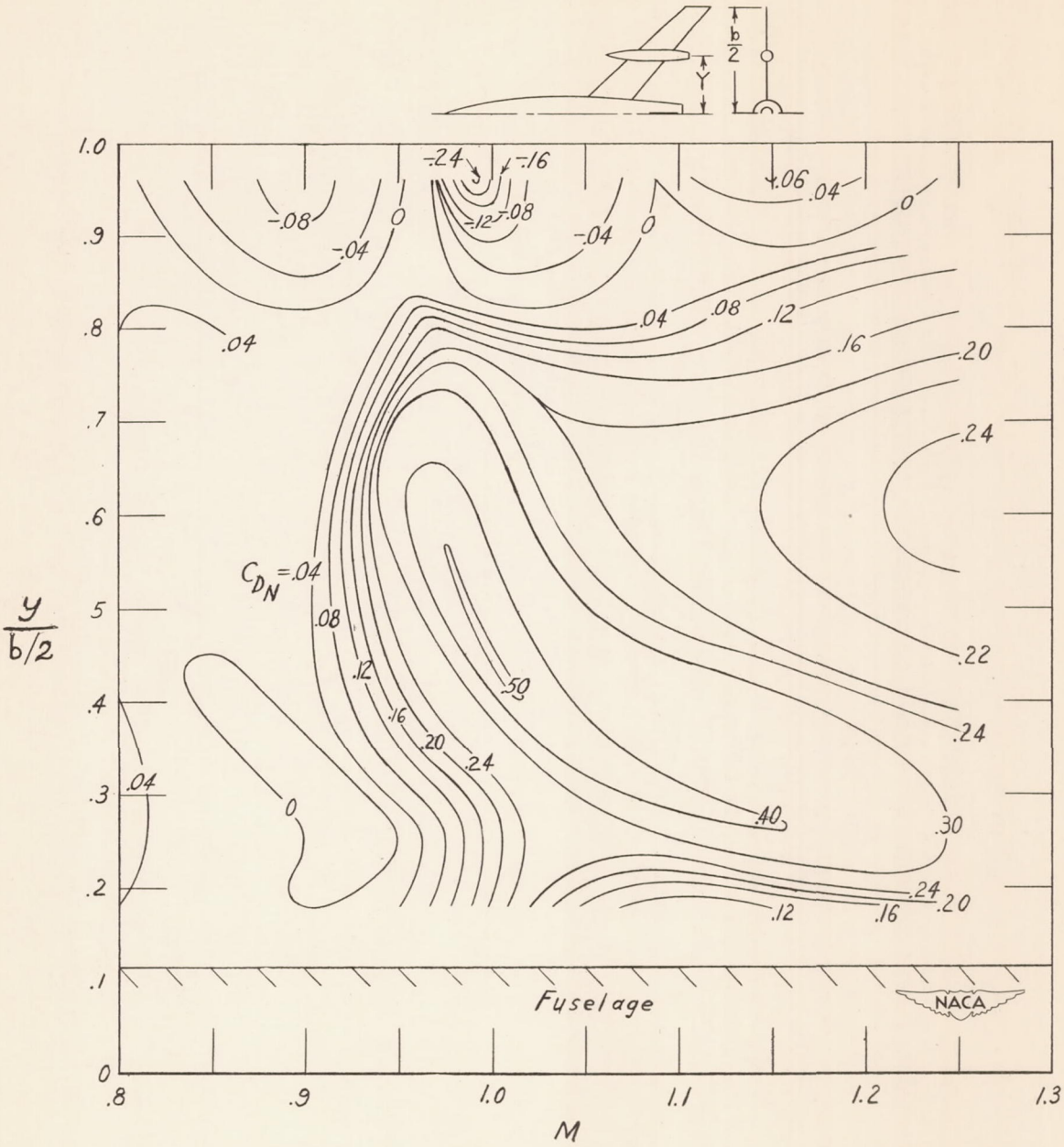

Figure 8.- Variation of nacelle-plus-interference drag coefficient with Mach number and spanwise nacelle position for symmetrically mounted nacelles with their points 50 percent of the nacelle length ahead of the wing maximum thickness.